The relationship between the magnetotelluric tensor invariants and the phase tensor of Caldwell, Bibby, and Brown

J.T. Weaver[1]   A.K. Agarwal[1]   F.E.M. Lilley[2]

Key Words: Magnetotelluric tensor, phase tensor, earth conductivity, Mohr circles

ABSTRACT

We examine the relationship between the seven invariants of the complex MT tensor, which we previously proposed as a vehicle for testing the dimensionality of the regional conductivity structure prior to an analysis of MT data, and the three invariants of the real 'phase tensor', recently introduced as an innovative aid in the treatment of MT data. It is found that the relevant invariants, and the necessary conditions on them for galvanically distorted data to be consistent with 1D, 2D, or 3D regional structures, agree in almost every detail for the two approaches. The new method does lead, however, to an improved normalisation of the eighth (dependent) invariant previously introduced. It is shown that the phase tensor can be expressed as a sum of three simple matrices, clearly associated with 1D, 2D and 3D regional conductivity structures respectively. It is further shown that it can be depicted graphically as a single Mohr circle that retains the principal properties of the separate real and imaginary Mohr circles associated with the MT tensor. The simplicity and elegance of the phase tensor method is achieved by dispensing with the capability of distinguishing between galvanically distorted and undistorted data in 1D and 2D regions, a distinction that is ultimately unimportant and unnecessary with real data. The paper concludes with a simple illustrative example of the theory applied to a real MT dataset from NE Australia. A shallow 1D regional conductivity structure associated with a sedimentary basin is revealed, and a 2D anomaly with calculated strike angle is also identified.

INTRODUCTION

In recent papers Caldwell, Bibby, and Brown (2002, 2004) (hereafter referred to as CBB) and Bibby et al. (2005) have introduced a new and elegant method for analysing magnetotelluric (MT) data which can be applied directly to galvanically distorted data in a regional conductivity structure of any dimension. It is therefore more general and direct than previous methods (e.g., Bahr, 1988; Groom and Bailey, 1989; Smith, 1995) which involve a decomposition of the MT tensor based on the assumption that the regional conductivity structure is 2D. The procedure of CBB, on the other hand, is founded on their innovative definition of a real 2×2 'phase tensor' which is independent of any real (galvanic) distortion that may be present (in fact it is identical for both the distorted and the regional data), and does not require any assumption about the dimensionality of the underlying regional conductivity.

Szarka and Menvielle (1997) and Weaver, Agarwal, and Lilley (2000) (WAL in the following) took a somewhat different approach by characterising the MT tensor in terms of different sets of seven independent invariants. WAL gave physical interpretations of each invariant in their chosen set, with the aim of finding necessary (but not sufficient) conditions for distinguishing between distorted and undistorted data and determining the dimensionality of the regional conductivity.

In this paper we examine how the MT tensor invariants of WAL that are associated with galvanically distorted data, are related to the properties of the CBB phase tensor. It is found that the seventh invariant of WAL, whose vanishing is necessary for the regional structure to be 2D, and whose magnitude otherwise indicates the degree of three-dimensionality, emerges quite naturally from the phase tensor in identical form. The conditions for the regional structure to be 1D, specified by WAL in terms of the vanishing of their sixth invariant and a supplementary dependent invariant, are also very similar when derived from the phase tensor. Only the normalisation of these two invariants is different in this case. The results are expressed concisely by writing the phase tensor as a sum of three matrices, each of which is obtained from the identity matrix by elementary operations and is multiplied by a factor proportional to one of the three relevant invariants. These three matrices are then clearly associated with 1D, 2D, and 3D conductivity structures respectively, and the relative magnitudes of their multiplying factors indicate the nature of the regional structure.

In contrast to CBB, who displayed the phase tensor graphically as an ellipse in the plane of the earth, we follow our previous practice with the MT tensor, by representing the phase tensor by its Mohr circle in the plane of the components in its first column. The three invariants of the real phase tensor are immediately identifiable in the Mohr circle diagram, with the conditions for 1D and 2D regional structures requiring the circle to shrink to a point, and to be centred on the horizontal axis, respectively. While these general properties are similar to those that hold for the separate real and imaginary Mohr circles associated with the MT tensor, identification of the seventh invariant of WAL is much more straightforward in the diagram for the phase tensor. It is proportional to the displacement of the centre of the Mohr circle from the horizontal axis, rather than being related in a rather complicated way to the coupling of the real and imaginary Mohr circles representing the MT tensor.

Finally, we illustrate the theory by applying it to a set of MT data obtained in the Mount Isa and Eromanga Basin region of NE Queensland in Australia. The invariant analysis clearly reveals a shallow 1D structure in the region of the sedimentary basin, and a 2D strike running roughly 26° east of north at one of the sites, which may be associated with the Carpentaria anomaly.

INVARIANTS OF THE MT TENSOR

The notation of WAL is introduced in this section. Later the ideas of CBB will be expressed in this notation, in order to facilitate comparison of their results with the magnetotelluric (MT) tensor invariants of WAL.

[1] *University of Victoria*
Department of Physics & Astronomy
Victoria, B.C., V8W 3P6
Canada

[2] *Australian National University*
Research School of Earth Sciences
Canberra, ACT 0200

In a rectangular coordinate system with x and y horizontal axes directed north and east respectively, and z vertically downwards into the earth, the MT tensor is represented by the 2×2 complex-valued matrix $\mathbf{M}$ defined by $\mathbf{e} = \mathbf{Mb}$ or

$$\begin{pmatrix} e_1 \\ e_2 \end{pmatrix} = \begin{pmatrix} M_{11} & M_{12} \\ M_{21} & M_{22} \end{pmatrix} \begin{pmatrix} b_1 \\ b_2 \end{pmatrix} , \tag{1}$$

where $\mathbf{e} = (e_1, e_2)^\mathrm{T}$ and $\mathbf{b} = (b_1, b_2)^\mathrm{T}$ are (complex-valued) column vectors representing the spatial parts of the horizontal electric and magnetic fields on the earth's surface. The time-dependence of these vectors is represented by a factor $\exp(i\omega t)$ which cancels out in the equation above. Real parameters ξ_j and η_j defined by

$$\xi_1 + i\eta_1 = (M_{11} + M_{22})/2, \quad \xi_2 + i\eta_2 = (M_{12} + M_{21})/2 \tag{2a}$$

$$\xi_3 + i\eta_3 = (M_{11} - M_{22})/2, \quad \xi_4 + i\eta_4 = (M_{12} - M_{21})/2 \tag{2b}$$

are introduced so that the matrix takes the form $\mathbf{M} = \mathbf{P} + i\mathbf{Q}$ where

$$\mathbf{P} = \begin{pmatrix} \xi_1 + \xi_3 & \xi_2 + \xi_4 \\ \xi_2 - \xi_4 & \xi_1 - \xi_3 \end{pmatrix}, \quad \mathbf{Q} = \begin{pmatrix} \eta_1 + \eta_3 & \eta_2 + \eta_4 \\ \eta_2 - \eta_4 & \eta_1 - \eta_3 \end{pmatrix}. \tag{3}$$

When the axes of measurement are rotated through an angle θ in a right-handed sense about the positive z-axis, as defined by the rotation matrix

$$\mathbf{R}(\theta) = \begin{pmatrix} \cos\theta & \sin\theta \\ -\sin\theta & \cos\theta \end{pmatrix} , \tag{4}$$

the matrix of the MT tensor in the rotated system is given by $\mathbf{R}(\theta) \mathbf{MR}^\mathrm{T}(\theta) = \mathbf{M}' = \mathbf{P}' + i\mathbf{Q}'$, where

$$\mathbf{P}' = \begin{pmatrix} \xi_1 + \xi_2 S + \xi_3 C & \xi_4 - \xi_3 S + \xi_2 C \\ -\xi_4 - \xi_3 S + \xi_2 C & \xi_1 - \xi_2 S - \xi_3 C \end{pmatrix} \tag{5a}$$

$$\mathbf{Q}' = \begin{pmatrix} \eta_1 + \eta_2 S + \eta_3 C & \eta_4 - \eta_3 S + \eta_2 C \\ -\eta_4 - \eta_3 S + \eta_2 C & \eta_1 - \eta_2 S - \eta_3 C \end{pmatrix} \tag{5b}$$

and $S = \sin 2\theta$ and $C = \cos 2\theta$.

It was shown by Szarka and Menvielle (1997) that Im(det $\mathbf{M}$) is an invariant under such rotations, which, as noted by WAL, is the same as stating that I, defined by

$$I = \xi_1 \eta_1 - \xi_2 \eta_2 - \xi_3 \eta_3 + \xi_4 \eta_4 \equiv \mathrm{Im}(\det \mathbf{M})/2 \neq 0 , \tag{6}$$

is invariant. It can be safely assumed that $I \neq 0$, for otherwise Im(det $\mathbf{M}$) vanishes, which renders the MT tensor physically meaningless. Szarka and Menvielle (1997) chose Im(det $\mathbf{M}$) as a fundamental member of their set of seven independent, rotational invariants defining the MT tensor. In the alternative scheme proposed by WAL, the first four invariants are

$$I_1 = (\xi_4^2 + \xi_1^2)^{1/2}, \quad I_2 = (\eta_4^2 + \eta_1^2)^{1/2}, \tag{7}$$

$$I_3 = (\xi_2^2 + \xi_3^2)^{1/2}/I_1, \quad I_4 = (\eta_2^2 + \eta_3^2)^{1/2}/I_2. \tag{8}$$

The three remaining invariants, defined in terms of the dimensionless parameters

$$d_{ij} = (\xi_i \eta_j - \xi_j \eta_i)/I , \quad s_{ij} = (\xi_i \eta_j + \xi_j \eta_i)/I , \tag{9}$$

are given by

$$I_5 = s_{41} I/(I_1 I_2), \quad I_6 = d_{41} I/(I_1 I_2), \quad I_7 = (d_{41} - d_{23})/I_0 , \tag{10}$$

where I_0, equivalent to $(Q I_1 I_2)/I$ in the notation of WAL, is a dependent invariant expressed by

$$I_0 = [(d_{12} - d_{34})^2 + (d_{13} + d_{24})^2]^{1/2} . \tag{11}$$

It is important to note that the definitions of d_{ij} and s_{ij} in (9) differ from the corresponding definitions of WAL, where the normalisation was by $I_1 I_2$ rather than I. This accounts for the factor $I/(I_1 I_2)$ appearing in the definitions of I_5 and I_6. All of the independent invariants except I_1 and I_2, which are based on the 'central impedances' introduced by Lilley (1993), were expressed as sines of real angles by WAL, so that their absolute values are bounded by 0 and 1.

The measured electric field can sometimes be regarded as an in-phase (or real) distortion of the *regional* electric field $\overline{\mathbf{e}}$. Such galvanic distortions are caused by charges accumulating on the boundary of a localised, near-surface, conductivity anomaly. The magnetic field of the electric currents associated with galvanic distortion is usually negligible compared with the regional magnetic field $\overline{\mathbf{b}}$. Thus we may assert that

$$\mathbf{e} = \mathbf{A}\overline{\mathbf{e}}, \quad \mathbf{b} = \overline{\mathbf{b}} , \tag{12}$$

where $\mathbf{A}$ is a (real) distortion matrix. Since the *regional* MT tensor $\overline{\mathbf{M}} = \overline{\mathbf{P}} + i\overline{\mathbf{Q}}$ is defined by $\overline{\mathbf{e}} = \overline{\mathbf{M}}\overline{\mathbf{b}} = \overline{\mathbf{M}}\mathbf{b}$, it follows that $\mathbf{Mb} = \mathbf{e} = \mathbf{A}\overline{\mathbf{e}} = \mathbf{A}\overline{\mathbf{M}}\mathbf{b}$, whence $\mathbf{M} = \mathbf{A}\overline{\mathbf{M}}$, or

$$\mathbf{P} = \mathbf{A}\overline{\mathbf{P}}, \quad \mathbf{Q} = \mathbf{A}\overline{\mathbf{Q}} , \tag{13}$$

since $\mathbf{A}$ is assumed real.

THE PHASE TENSOR

In a recent paper, CBB introduced a 'phase tensor' represented here by the 2×2 *real* matrix $\mathbf{T}$, and defined by

$$\mathbf{T} = \mathbf{P}^{-1}\mathbf{Q} . \tag{14}$$

An important property of this tensor is that in the presence of in-phase distortion

$$\mathbf{T} = \mathbf{P}^{-1}\mathbf{Q} = (\mathbf{A}\overline{\mathbf{P}})^{-1}\mathbf{A}\overline{\mathbf{Q}} = \overline{\mathbf{P}}^{-1}\mathbf{A}^{-1}\mathbf{A}\overline{\mathbf{Q}} = \overline{\mathbf{P}}^{-1}\overline{\mathbf{Q}} = \overline{\mathbf{T}} . \tag{15}$$

In other words, the phase tensor is the same for both the regional field and the locally distorted field. Moreover, CBB showed that when the regional conductivity structure is two-dimensional (2D), so that the diagonal elements of $\overline{\mathbf{P}}$ and $\overline{\mathbf{Q}}$ vanish in the strike frame whose axes are aligned along and perpendicular to the direction of the regional strike, then $\mathbf{T}$ is necessarily symmetric. For when the axes are rotated into the strike frame, $\overline{\mathbf{T}}' = (\overline{\mathbf{P}}')^{-1}\overline{\mathbf{Q}}'$ becomes diagonal, taking the form

$$\overline{\mathbf{T}}' = \begin{pmatrix} \overline{Q}'_{21} / \overline{P}'_{21} & 0 \\ 0 & \overline{Q}'_{12} / \overline{P}'_{12} \end{pmatrix}, \tag{16}$$

and since symmetry is preserved under a rotation (4), $\overline{\mathbf{T}}$ is also symmetric in the frame of measurement. It follows at once from (15) that $\mathbf{T}$ is symmetric in the frame of measurement as well. Thus symmetry of the phase tensor is an immediate and simple indication that MT data, whether locally distorted or not, are consistent with a 2D regional conductivity structure. Furthermore, it follows from (16) that when $\mathbf{T}$ is symmetric, $\mathbf{T}' = \overline{\mathbf{T}}'$ becomes diagonal in the strike frame, thereby enabling an expression for the regional strike angle to be derived.

If the regional structure is 1D, i.e., the conductivity varies only with depth, then we require

$$\bar{P}_{12} = -\bar{P}_{21} = \bar{P} \quad \text{and} \quad \bar{Q}_{12} = -\bar{Q}_{21} = \bar{Q}$$

(say) for all angles of rotation. Hence (15) and (16) give

$$\mathbf{T} = \bar{\mathbf{T}} = \mathbf{I}\tan\varphi \ , \tag{17}$$

where $\mathbf{I}$ is the identity matrix and $\varphi = \arctan(\bar{Q}/\bar{P})$ is the familiar impedance phase of the 1D regional structure.

COMPARISON WITH THE MT INVARIANTS

As shown by CBB, the phase tensor can be readily expressed directly in terms of the components of the MT tensor itself. However, in order to facilitate a comparison with previous results, the notation and invariants of WAL introduced earlier are preferred here. Substituting from (3) into (14), and inverting $\mathbf{P}$, we note that

$$\mathbf{T} = \frac{1}{\xi_1^2 - \xi_2^2 - \xi_3^2 + \xi_4^2} \times$$
$$\begin{pmatrix} \xi_1 - \xi_3 & -\xi_2 - \xi_4 \\ -\xi_2 + \xi_4 & \xi_1 + \xi_3 \end{pmatrix} \begin{pmatrix} \eta_1 + \eta_3 & \eta_2 + \eta_4 \\ \eta_2 - \eta_4 & \eta_1 - \eta_3 \end{pmatrix}.$$

Introducing an invariant quantity J_1 defined by

$$J_1 = \frac{\xi_1\eta_1 - \xi_2\eta_2 - \xi_3\eta_3 + \xi_4\eta_4}{\xi_1^2 - \xi_2^2 - \xi_3^2 + \xi_4^2} \equiv \frac{I_1}{I_1^2\left(1 - I_3^2\right)} \ , \tag{18}$$

and performing the matrix product with the aid of definitions (9), we obtain

$$\mathbf{T} = J_1\begin{pmatrix} 1 + d_{13} + d_{24} & d_{12} - d_{34} - d_{41} + d_{23} \\ d_{12} - d_{34} + d_{41} - d_{23} & 1 - d_{13} - d_{24} \end{pmatrix}. \tag{19}$$

Under a rotation of axes (4), the matrix $\mathbf{T}$ in (19) transforms into

$$\mathbf{T}' = J_1\begin{pmatrix} 1 + d_{1324}C + d_{1243}S & d_{1243}C - d_{1324}S - I_0I_7 \\ d_{1243}C - d_{1324}S + I_0I_7 & 1 - d_{1324}C - d_{1243}S \end{pmatrix}, \tag{20}$$

where we have substituted from the last equation in (10), and for convenience, have defined $d_{ijkl} \equiv d_{ij} + d_{ki}$.

It follows from (20) that the condition for $\mathbf{T}$ to be symmetric is $I_0I_7 = 0$ (or $d_{41} = d_{23}$), and furthermore that $\mathbf{T}$ becomes diagonal when the axes are rotated through an angle $\theta = \theta_s$, satisfying $d_{1243}C = d_{1324}S$, i.e.,

$$\tan 2\theta_s = \frac{d_{1243}}{d_{1324}} \equiv \frac{d_{12} + d_{43}}{d_{13} + d_{24}} = \frac{d_{12} - d_{34}}{d_{13} + d_{24}} \ . \tag{21}$$

Equation (19) can now be expressed more concisely in terms of θ_s as

$$\mathbf{T} = J_1\begin{pmatrix} 1 + I_0\cos2\theta_s & I_0\sin2\theta_s - I_0I_7 \\ I_0\sin2\theta_s + I_0I_7 & 1 - I_0\cos2\theta_s \end{pmatrix}. \tag{22}$$

If the regional structure is 1D then, in accordance with (17), $\mathbf{T}$ must reduce to the identity matrix multiplied by some scalar. Thus the required conditions are $I_0I_7 = d_{41} - d_{23} = 0$ and $I_0 = 0$, since they reduce equation (22) to (17) with $\tan\varphi = J_1$. The measured data are then consistent with a 1D regional structure with impedance phase given by this value of φ. It also follows from (22) that $I_0I_7 = 0$ ($I_0 \neq 0$) is the necessary condition for a 2D regional structure and that the strike angle is θ_s defined by (21), the same result obtained by WAL and earlier by Bahr (1988).

Defining

$$\mathbf{K}_1 = \begin{pmatrix} 1 & 0 \\ 0 & -1 \end{pmatrix} \quad \mathbf{K}_2 = \begin{pmatrix} 0 & 1 \\ 1 & 0 \end{pmatrix} \quad \mathbf{K} = \begin{pmatrix} 0 & -1 \\ 1 & 0 \end{pmatrix}, \tag{23}$$

and $\mathbf{J} = \mathbf{K}_1\cos2\theta_s + \mathbf{K}_2\sin2\theta_s$, we can make these observations more transparent by rewriting (22) in the form

$$\mathbf{T} = J_1\mathbf{I} + J_2\mathbf{J} + J_3\mathbf{K} \ , \tag{24}$$

where

$$J_2 = I_0J_1 \ , \quad J_3 = I_7J_2 \ . \tag{25}$$

The first, second, and third terms in (24) can then be regarded as the 1D, 2D and 3D contributions to the phase tensor respectively, and their magnitudes are in the ratios $1 : I_0 : I_0|I_7|$.

From its definition (11), it is obvious that $I_0 = 0$ if and only if $d_{12} - d_{34} = 0$ and $d_{13} + d_{24} = 0$. Indeed, these conditions ensure that both numerator and denominator of (21) vanish when $I_0 = 0$, thereby rendering θ_s indeterminate, as required when the structure is 1D. It follows that the left-hand side of the identity

$$\left(s_{13} - s_{24}\right)\left(d_{12} - d_{34}\right) - \left(s_{12} + s_{24}\right)\left(d_{13} + d_{24}\right) \equiv$$
$$d_{41}\left(s_{22} + s_{33}\right) - d_{23}\left(s_{44} + s_{11}\right)$$

(WAL, equation (31)) vanishes when $I_0 = 0$, and since by definitions (6) and (9) we have $s_{44} + s_{11} - s_{22} - s_{33} = 2$, the other condition for a 1D regional structure, $d_{41} = d_{23}$, further implies that $d_{41} = d_{23} = 0$. Hence $(I_1I_2/I)I_6 \equiv d_{41} = d_{23} = 0$. Thus, in complete agreement with the criteria specified by WAL, the conditions for local distortion in a 1D region are satisfied when $I_6 = I_0 = 0$, in which case I_7 becomes indeterminate because $d_{41} = d_{23} = 0$ when $I_0 = 0$. It was observed by WAL that the same conditions arise when there is local distortion in a 2D region at a position where there is no phase splitting between the E-polarization and B-polarization fields.

Conditions for 1D Structures in Practice

With real data, the invariants will never vanish precisely; rather, they will become negligibly small in some sense. Thus for an interpretation of regional one-dimensionality we want the second and third terms in (24) to be always negligibly small compared with the first term. These conditions will hold provided that $J_1I_0|\cos2\theta_s|$, $J_1I_0|\sin2\theta_s|$ and $J_1I_0|I_7|$ are all very much less than J_1. In other words, we require

$$I_0 \ll 1, \quad I_0|I_7| \equiv |d_{41} - d_{23}| \ll 1 \ . \tag{26}$$

Thus the practical criteria for assuming that MT data are consistent with a 1D regional structure are $|d_{41} - d_{23}| < 0.1$ to maintain the symmetry of $\mathbf{T}$, and $I_0 < 0.1$ to ensure that $\mathbf{T}$ is approximately a scalar multiple of the identity matrix. These conditions are similar to those prescribed by WAL except for the different normalisation of the parameters d_{ij}. This normalisation has led to a proper justification of the first criterion in (26), compared with the rather more speculative assertion $Q < 0.1$ made by WAL in the original notation.

Conditions for 2D Structures in Practice

Likewise, for an interpretation of regional two-dimensionality we may assert that the elements of the antisymmetric part of $\mathbf{T}$, which are clearly invariant under a rotation of the axes, must always be small in magnitude compared with the corresponding

off-diagonal elements in the symmetric part, which are not invariant. It is immediately apparent from equation (22) that the required condition is

$$I_0|I_7| \ll I_0|\sin 2\theta_s| \le I_0, \quad \text{i.e. } |I_7| \ll 1 , \tag{27}$$

which, by (25), is equivalent to $|J_3| \ll |J_2|$ in (24). Thus a reasonable criterion in practice for a 2D interpretation of the regional conductivity structure is $|I_7| < 0.1$. This is precisely the necessary condition obtained by WAL using different arguments. As mentioned in Section 1, it was also shown by WAL that if $|I_7|$ exists, then $|I_7| \le 1$. When $|I_7| > 0.1$, it is concluded that the regional structure is 3D, the degree of three-dimensionality increasing with $|I_7|$.
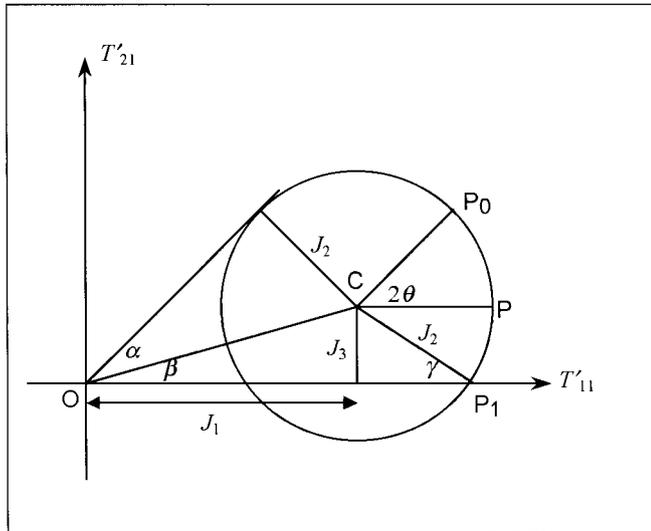

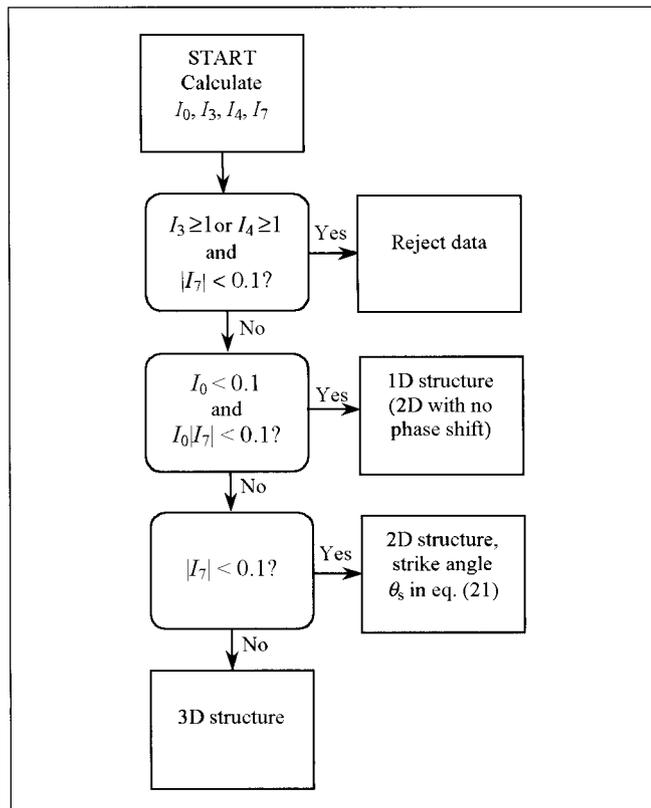**Fig. 1. Mohr circle representation of the phase tensor.**

Fig. 2. Flow chart for analysis of MT data.

MOHR CIRCLE FOR THE PHASE TENSOR

Following Bibby (1986), CBB displayed the phase tensor graphically as an ellipse in the xy-plane. An alternative approach, adopted here as an aid to the discussion of tensor invariants, is to represent the phase tensor by a Mohr circle (Lilley, 1993) drawn in the plane of T'_{11} and T'_{21}.

The three independent invariants J_1, J_2, and J_3 defined in (18) and (25) are related, respectively, to the determinant, the trace, and the 'skew' (the difference of its off-diagonal elements) of the phase tensor, which are the three well-known independent invariants of a 2×2 matrix under rotations. Then we obtain from (22) and (25)

$$(T'_{11} - J_1)^2 + (T'_{21} - J_3)^2 = J_2^2 , \tag{28}$$

which is the circle with centre (J_1, J_3) and radius J_2 traced out by the point (T'_{11}, T'_{21}), or P in Figure 1, as θ varies. The starting point of P, denoted by P_0 in Figure 1, represents the recorded values of the MT tensor components in the actual axes of measurement. When the axes (x, y) are rotated through an angle θ in the right-handed sense about the positive z-axis, P moves from P_0 clockwise around the circle through an angle 2θ.

From the preceding analysis it is readily seen that if the regional conductivity structure is 2D, then $J_3 = 0$, i.e., the centre of the Mohr circle lies on the horizontal axis $T'_{21} = 0$. The strike direction is reached when P is on the horizontal axis as it rotates around the circle, the strike angle θ_s being given by half its angle of rotation.

The more realistic condition (27) translates into $|J_3| \ll J_2$, or $|\sin \gamma| < 0.1$ where γ is the angle shown in Figure 1. If the regional structure is 3D, then $|J_3| / J_2 > 0.1$. Note that when γ is small, but non-vanishing, the strike angle given by (21) corresponds to the point P on the Mohr circle where T'_{11} attains its extremum value $J_1 + J_2$, i.e., where CP is horizontal as depicted in Figure 1, not the point P_1 where it intersects with the horizontal axis. Thus the off-diagonal elements of $\mathbf{T}'$ are not equal to zero when $\theta = \theta_s$ in this case, nor do they vanish simultaneously at any point, but rather vanish individually for the two distinct angles of rotation

$$\theta = \theta_s \pm (\arcsin I_7)/2 . \tag{29}$$

Hence $(\arcsin I_7)/2$ can be regarded as a measure of the uncertainty in the strike angle given by (21) with real data.

If the regional conductivity is 1D, then $J_2 = J_3 = 0$ and the Mohr circle shrinks to a point on the horizontal axis. In practical terms, the relevant conditions corresponding to (26) are $J_2 \ll |J_1|$ and $|J_3| \ll |J_1|$. Since $|J_1| \le (J_1^2 + J_3^2)^{1/2}$, the conditions for a 1D interpretation of the data to hold can be expressed geometrically as $|\sin \alpha| \ll 1$ and $|\sin \beta| \ll 1$, where α and β are the angles shown in Figure 1.

It is concluded, therefore, that three invariants, $|J_3|/J_2 \equiv |I_7|$, $J_2/|J_1| \equiv I_0$, and $|J_3/J_1| \equiv I_0|I_7| \equiv |d_{41} - d_{23}|$, which are based on just two (rather than seven) independent invariants, I_0 and I_7, of the original MT tensor, can be used as indicators of the dimensionality of the regional structure. All three are less than or equal to sines of angles in the Mohr circle diagram, are therefore bounded by 0 and 1, and can be considered small when they are less than 0.1 in magnitude.

The Mohr circle representation and decomposition (24) can be compared with the corresponding procedures used by CBB to display the phase tensor graphically and reveal the role played by its invariants. By analogy with the method of Bibby (1986) for representing the DC apparent resistivity tensor, they portrayed

the phase tensor as an ellipse in the xy-plane, given in polar coordinates (r, ψ) by

$$\frac{r^2\cos^2(\psi - \theta_s - \beta/2)}{(J_0 + J_2)^2} + \frac{r^2\sin^2(\psi - \theta_s - \beta/2)}{(J_0 - J_2)^2} = 1 , \qquad (30)$$

where $J_0 = (J_1^2 + J_3^2)^{1/2}$ and β is the angle shown in Figure 1, defined by $\tan\beta = J_3/J_1$. Here the polar radius r in the direction defined by the unit vector $\mathbf{n} \equiv \mathbf{r}/|\mathbf{r}|$, is related to $\mathbf{T}$ by the formula $1/r = |\mathbf{T}^{-1} \cdot \mathbf{n}|$. It is at once apparent from the form of (30) that the lengths of the semi-major and semi-minor axes of the ellipse are given by $J_0 + J_2$ and $J_0 - J_2$ respectively, and that the major axis is rotated through a positive angle $\theta_s + \beta/2$ from the x-axis in the observer's frame. If the regional structure is 1D, the ellipse reduces to a circle of radius $J_1 \equiv \tan\varphi$ where φ is the impedance phase. If the region is 2D, then $\mathbf{T}$ is symmetric so that $J_3 = 0$, i.e., $\beta = 0$, and the axes of the ellipse lie along and perpendicular to the direction of strike.

Routine algebra verifies that the matrix representing $\mathbf{T}$ in (22) can be decomposed into the form

$$\mathbf{T} = \mathbf{R}^T(\theta_s + \beta/2)\,\mathbf{diag}\,(J_0 + J_2,\ J_0 - J_2)\,\mathbf{R}(\theta_s - \beta/2) , \qquad (31)$$

where $\mathbf{R}$ is the rotation matrix (4) and $\mathbf{diag}(a, b)$ is the 2×2 diagonal matrix with elements a and b. This is essentially the singular value decomposition of $\mathbf{T}$ employed by CBB, albeit in a different notation. It expresses the dependence of $\mathbf{T}$ on the three invariants J_1, J_2, and J_3 and the angle θ_s rather differently from that in the previous decomposition (24).

DISCUSSION

While the conclusions reached about the nature of MT data are generally similar whether they are based on the invariants of the MT tensor itself, or on the phase tensor of CBB, there is little doubt that the innovative and insightful approach of CBB leads to a more elegant and much simpler analysis, largely because the phase tensor is real whereas the MT tensor is complex. Thus there are only three tensor invariants to consider compared with the seven invariants of the MT tensor, and they can be displayed geometrically with the aid of only one Mohr circle compared with the two coupled Mohr circles required for the MT tensor. An interesting outcome of the analysis is that the dependent invariant I defined in (6), has emerged as a more natural normalizing factor when defining the parameters d_{ij} and s_{ij} than the term $I_1 I_2$ chosen by WAL.

The gains in simplicity achieved by employing the phase tensor of CBB can only be won, of course, with sacrifices made elsewhere. What has been lost is the ability to distinguish between distorted and undistorted data in 2D and 1D regions, although this information is still available, of course, in the full complex MT tensor. This is a minor penalty to pay, however, because real data are always distorted in some sense, and strictly 2D or 1D configurations are only found in idealised mathematical models, not in the real world. In fact, some of the results for truly 2D or 1D conductivity structures are already included in the corresponding results for distorted data. Thus, if the regional structure is 2D and the data are undistorted, then there exists an angle θ_s such that $P'_{11} = P'_{22} = Q'_{11} = Q'_{22} = 0$, i.e., from (5)

$$\xi_1 = \eta_1 = 0, \quad \tan 2\theta_s = -\xi_3/\xi_2 = -\eta_3/\eta_2 , \qquad (32)$$

as stated by WAL. The first of these conditions reduces the formula (21), and the condition $I_0 I_7 = 0$ for the phase tensor to be symmetric, to $\tan(2\theta_s) = -d_{34}/d_{24}$ and $d_{23} = 0$ respectively. It follows by simple algebra that (21) then simplifies to the expression in

Site	1	2	3	4	5	6	7	8	9	10
T (s)										
.006	I	+	—	—	+	+	+	—	—	—
.008	I	I	—	—	+	—	+	—	—	—
.012	I	I	I	—	+	—	—	—	—	—
.018	+	+	+	—	+	—	—	—	—	+
.026	+	+	I	—	—	—	—	—	—	+
.029	+	+	I	—	I	—	—	—	—	—
.041	+	+	I	—	I	—	—	—	—	—
.058	+	+	I	—	I	I	+	—	—	—
.068	+	+	I	I	+	+	I	—	—	—
.083	+	+	I	+	I	+	+	—	—	—
.114	+	+	+	+	+	+	+	+	—	+
.120	+	+	I	+	I	I	I	—	—	—
.177	+	+	I	+	+	I	I	—	—	—
.263	+	+	I	+	+	I	I	—	—	—
.293	+	+	+	+	+	+	+	—	+	—
.410	+	+	I	+	+	+	+	—	+	+
.580	+	+	+	+	+	+	+	+	+	—
.683	+	+	+	—	+	+	I	+	+	—
.819	+	I	I	+	+	+	+	+	+	+
1.14	+	+	+	+	+	+	+	+	—	+
1.67	+	+	I	+	+	+	+	+	—	+
2.41	+	+	—	+	+	+	+	+	—	+
3.53	+	+	I	+	+	+	I	+	+	+
5.25	+	+	+	+	+	+	+	+	+	+
7.43	+	+	+	+	—	—	+	+	+	+
8.19	+	+	I	+	+	+	+	+	+	+
10.4	+	+	+	+	+	+	+	+	+	+
13.7	+	+	+	+	+	+	+	+	+	+
20.6	+	—	+	+	I	+	I	+	+	+
29.0	+	—	+	+	+	+	+	+	+	I
41.0	+	—	+	+	I	+	+	+	+	+
83.3	+	—	+	+	I	+	+	+	+	I
175	+	+	+	+	+	+	+	+	+	+
416	+	+	+	+	+	+	+	+	+	
1110	+	+	+	+	+	+	+	+	+	—

Table 1. Schematic diagram showing the interpretation of the conductivity structure, 1D (–), 2D (|) or 3D (+), at selected sites and for each period, as given by the tensor invariants. A blank cell indicates a rejected datum. The sites are numbered from west to east, with geographical coordinates: 1 (20.70°S, 140.30°E), 2 (20.72°S, 140.62°E), 3 (20.67°S, 140.82°E), 4 (20.64°S, 140.93°E), 5 (20.64°S, 141.00°E), 6 (20.63°S, 141.10°E), 7 (20.62°S, 141.20°E), 8 (20.65°S, 141.41°E), 9 (20.64°S, 141.54°E), 10 (20.66°S, 141.71°E). The rows are ordered from top to bottom with increasing period T in seconds.

Period T (s)	Site 3	Site 5
0.012	24.9° ± 1.2°	
0.018	27.5° ± 3.8°	
0.026	24.7° ± 0.4°	
0.029	26.3° ± 2.2°	30.8° ± 0.5°
0.041	27.3° ± 2.4°	29.1° ± 1.8°
0.058	27.7° ± 1.9°	28.7° ± 1.1°
0.068	26.5° ± 2.2°	23.9° ± 4.3°
0.083	26.8° ± 0.1°	29.2° ± 1.1°
0.114	25.0° ± 4.0°	38.5° ± 7.1°
0.120	24.9° ± 2.3°	30.4° ± 1.5°
0.177	19.9° ± 0.7°	29.8° ± 4.8°
0.263	17.1° ± 1.7°	29.4° ± 4.7°

Table 2. Strike angles and their uncertainties.

(32). For a 1D structure without distortion, we have additionally $P'_{12} = -P'_{21}$ and $Q'_{12} = -Q'_{21}$, whence $\xi_2 = \eta_2 = \xi_3 = \eta_3 = 0$ as well. Thus the phase tensor (19) reduces to $\mathbf{T} = J_1\mathbf{I} = (\eta_4/\xi_4)\mathbf{I} = (I_2/I_1)\mathbf{I}$, which by comparison with (17), shows that the impedance phase of the 1D region is given by $\arctan(I_2/I_1)$, in agreement with a result quoted by WAL. The associated apparent resistivity was also stated by WAL to be $\mu_0(I_1^2 + I_2^2)/\omega$, where μ_0 is the permeability of free space, but this information is not recoverable when dealing with the phase tensor alone.

A SIMPLE ANALYSIS OF DATA

Following the scheme illustrated in Figure 2, we have applied the ideas described above to a rudimentary analysis of MT data collected in a region of NE Australia. Note that the flow chart rejects those measurements that appear not to be 3D (i.e., $|I_7| <$ 0.1) and yet violate the conditions det(Re $\mathbf{M}$) > 0 and det(Im $\mathbf{M}$) > 0 suggested by Lilley (1998) as necessary for physical MT data to be treatable. Such data do occasionally occur in practice, and are possibly associated with a high degree of local (as distinct from regional) anisotropy.

The data were collected in NW Queensland at MT sites along a line from Mount Isa in the west to the Eromanga Basin in the east. The line traverses the Carpentaria anomaly (Chamalaun et al., 1999), which runs roughly north-south and may mark the boundary between the pre-Cambrian Mount Isa block and the younger rocks of the basin. The data were supplied as components of the *impedance* tensor $\mu_0\mathbf{M}$ measured in mV/km/nT for periods T in the range 6.0×10^{-3} s to 1.11×10^3 s.

Mean values of the tensor components with their standard errors were available for each site and period. For this preliminary demonstration of the preceding theory applied to field data, we have simply computed the invariants and strike angles (where relevant) for a range of periods at 10 selected sites, from the mean values of the tensor components. Three distinctive symbols are used in Table 1 to show the interpretation of the data at each site as suggested by the values of the tensor invariants. Horizontal and vertical lines represent 1D and 2D structures respectively, while a combination of the two (a plus sign) represents a 3D region. The relevant symbols for each site are displayed in a column in order of increasing period from top to bottom, and the columns themselves are arranged alongside each other from left to right corresponding to the order of sites from west to east along the profile. The resulting diagram as such is only schematic; the columns and rows are equally spaced, even though neither the distance between the actual sites nor the interval between the square root of the measured periods are uniform. Nevertheless it is useful in providing an immediate visualization of the regional structure.

The sedimentary basin is revealed as a 1D region near the surface on the right of the profile, whereas the Mount Isa block on the left has a mainly 3D interpretation. The data at Site 3, and to a lesser extent at Site 5, are consistent with a shallow 2D structure over a range of periods, and probably reflect the presence of the Carpentaria anomaly. Table 2 displays the values of strike angle at these two sites as calculated from formula (21), along with their theoretical uncertainties as given by (29). The calculated strike angles are, of course, ambiguous to the extent of ±90°. Where the value of $|I_7|$ unexpectedly suggests a 3D structure at a single period within a range that is otherwise 2D (e.g., period 0.114 s at Site 3), we have calculated a strike angle anyway, because the cut-off value of 0.1, which distinguishes 2D from 3D regions, is somewhat arbitrary. The larger value of $|I_7|$ in such cases is always reflected in the increased uncertainty in the calculated value of the strike angle.

For the 10 periods in the range 1.2×10^{-2} s to 1.2×10^{-1} s, the average strike angle at Site 3 is N26.2°E with a standard deviation of 1.1°. If the last two results for Site 3, up to the period 2.63×10^{-1} s, are taken into account, the average strike angle becomes N24.9°E with a much larger standard deviation of 3.1°. The average strike direction determined from 9 periods in the same period range at Site 5 is N30.0°E with standard deviation 3.6°. These results compare quite well with the strike angle determined by Groom-Bailey decomposition for short periods on the west of the profile (Lilley et al., 2003).

Since the conditions for determining the dimensionality of the regional conductivity are necessary, but not sufficient, we have ignored the occasional isolated examples in Table 1 indicating a 1D or 2D structure. If the region were truly 1D or 2D then we would expect this to be seen over a range of periods, especially if only in-phase distortion is present, as assumed in the theory.

Finally, we emphasise that the above example of treating real data is primarily illustrative to demonstrate an application of the theory in practice, not to present a detailed, thorough investigation of the Australian data. A full treatment would include an error analysis based on the given standard errors of the MT tensor components. It is hoped eventually to present such an analysis of these and other MT data elsewhere.

CONCLUSIONS

By employing the phase tensor of Caldwell, Bibby, and Brown (2002, 2004), we have greatly simplified and clarified our earlier investigation of the MT tensor invariants and their application to an interpretation of MT data. In place of the seven independent invariants (plus one additional dependent invariant which proved useful in the previous study), only three are needed to characterise the real phase tensor, which nevertheless retains the salient properties of the more familiar, but complex, MT tensor with virtually no loss of insight. It has been shown that the necessary conditions on these three invariants for the regional conductivity structure to be 1D, 2D, or 3D are essentially equivalent to those we derived in our previous paper for galvanically distorted data. The previous dependent invariant, however, has now been renormalised and is related to one of the three independent invariants, J_2. This leads to a more satisfactory understanding of its role in the interpretation of MT data, and graphically it is clearly seen to be proportional to the radius of the Mohr circle for the phase tensor. Likewise, I_7 is now readily identified as being proportional to the off-axis displacement of the Mohr circle, whereas in our earlier paper it was related in an obscure way to an angle that served as the coupling between the two Mohr circles representing the separate real and imaginary parts of the MT tensor.

The simplicity of the new approach is embodied in equation (24), which separates the phase tensor into three simple matrices associated with 1D, 2D, and 3D structures, respectively. The 2D and 3D terms are multiplied by factors involving those invariants that were shown in our earlier work to be necessarily vanishing when the regional structure is 1D, while the factor in the third term was similarly shown to vanish alone when the regional structure is 2D. Thus the decomposition summarised by equation (24) is somewhat different from that favoured by CBB who diagonalised the phase tensor by a singular value decomposition involving the strike angle θ_s and a 'skew angle' given by $-\beta/2 \equiv [\arctan(-I_0 I_7)]/2$ in our notation.

Although the map of regional dimensionality in Table 1 is very similar to that obtained when we examined the Australian data (Agarwal, Weaver and Lilley, 2000) according to the criteria given by WAL, some of the strike angles computed at '2D sites' are quite different. This is because the previous analysis distinguished between apparently distorted and undistorted data at 2D sites, and prescribed different formulae, (21) for the former and a modified form of (32) for the latter, for calculating the strike angle in the two cases. When using equation (32) we make the tacit assumption that $d_{23} \approx 0$. Theoretically the vanishing of d_{23}, which is equivalent to $I_7 = I_6 = 0$, is indeed a requirement for a 2D structure. A re-examination of the data, however, showed that even when both conditions $I_7 < 0.1$ and $I_6 < 0.1$ were satisfied, it did not always follow that d_{23} was negligible. In such cases, the angles given by the two alternative formulae in (32) can be significantly different,

and their average value $-s_{23}/s_{22}$, which was actually used by WAL to calculate the strike angle, then becomes unreliable. An advantage of a method based on the phase tensor of CBB is that distorted and undistorted data are treated alike, so that the formula for the strike angle given in (21) is always used. As we have shown, this formula reduces algebraically to (32) when $d_{23} = 0$.

The analysis of noisy synthetic data undertaken by WAL showed that computed values of the strike angle given by (21) and the invariant I_7 defined in (10), were less stable than the values obtained for the other invariants. A detailed treatment of the Australian and other MT data must therefore include an error analysis based on the standard errors of the MT tensor components in order to place some confidence limits on calculated strike angles.

ACKNOWLEDGMENTS

REFERENCES

Agarwal, A.K., Weaver, J.T., and Lilley, F.E.M., 2000, An application of tensor invariant analysis to real data: *15th Workshop on Electromagnetic Induction in the Earth*, Cabo Frio, Brazil, Abstract EM12–4.

Bahr, K., 1988, Interpretation of the magnetotelluric impedance tensor: regional induction and local telluric distortion: *Journal of Geophysics*, **62**, 119–127.

Bibby, H.M., 1986, Analysis of multiple-source bipole- quadrupole resistivity surveys using the apparent resistivity tensor: *Geophysics*, **51**, 972–983.

Bibby, H.M., Caldwell, T.G., and Brown, C., 2005, Determinable and non-determinable parameters of galvanic distortion in magnetotellurics: *Geophysical Journal International*, **163**, 915–930.

Caldwell, T.G., Bibby, H.M., and Brown, C., 2002, The magnetotelluric phase tensor – a method of distortional analysis for 3D regional conductivity structures: *16th Workshop on Electromagnetic Induction in the Earth, Santa Fe, New Mexico, USA*, Abstract EM12–4.

Caldwell, T.G., Bibby, H.M., and Brown, C., 2004, The magnetotelluric phase tensor: *Geophysical Journal International*, **158**, 457–469.

Chamalaun, F.H., Lilley, F.E.M., and Wang, L.J., 1999, Mapping the Carpentaria conductivity anomaly in northern Australia: *Physics of the Earth and Planetary Interiors*, **116**, 105–115.

Groom, R.W., and Bailey, R.C., 1989, Decomposition of the magnetotelluric tensors in the presence of local three-dimensional galvanic distortion: *Journal of Geophysical Research*, **94**, 1913–1925.

Lilley, F.E.M., 1993, Magnetotelluric analysis using Mohr circles: *Geophysics*, **58**, 1498–1506.

Lilley, F.E.M., 1998, Magnetotelluric tensor decomposition: Part 1. Theory for a basic procedure: *Geophysics*, **63**, 1885–1897.

Lilley, F.E.M., Wang, L.J., Chamalaun, F.H., and Ferguson, I.J., 2003, The Carpentaria electrical conductivity anomaly, Queensland, as a major structure in the Australian plate: in Hillis, R. and Mueller, D. (eds), *The evolution and dynamics of the Australian plate*: Joint Special Publication of the Geological Society of Australia and the Geological Society of America, 141–156.

Smith, J.T., 1995, Understanding telluric distortion matrices: *Geophysical Journal International*, **122**, 219–226.

Szarka, L., and Menvielle, M., 1997, Analysis of rotational invariants of the magnetotelluric impedance tensor: *Geophysical Journal International*, **129**, 133–142.

Weaver, J.T., Agarwal, A.K., and Lilley, F.E.M., 2000, Characterization of the magnetotelluric tensor in terms of its invariants: *Geophysical Journal International*, **141**, 321–336.